TROPOMI NO_2 in the United States: A detailed look at the annual averages, weekly cycles, effects of temperature, and correlation with $PM_{2.5}$

Daniel L. Goldberg*[,1,2], Susan C. Anenberg[1], Arash Mohegh[1], Zifeng Lu[2], David G. Streets[2]

[1]Department of Environmental and Occupational Health, George Washington University, Washington, DC 20052, U.S.

[2]Energy Systems Division, Argonne National Laboratory, Argonne, IL 60439, U.S.

*Corresponding author. Phone: (202)994-8102; Email: dgoldberg@gwu.edu

Abstract

Observing the spatial heterogeneities of NO_2 air pollution is an important first step in quantifying NO_X emissions and exposures. This study investigates the capabilities of the Tropospheric Monitoring Instrument (TROPOMI) in observing the spatial and temporal patterns of NO_2 pollution in the Continental United States (CONUS). The high instrument sensitivity can differentiate the fine-scale spatial heterogeneities in urban areas, such as hotspots related to airport/shipping operations and high traffic areas, and the relatively small emission sources in rural areas, such as power plants and mining operations. We also examine NO_2 columns by day-of-the-week and find that Saturday and Sunday concentrations are 16% and 24% lower respectively than during weekdays. In cities with topographic features that inhibit dispersion, such as Los Angeles, there appears to be a pollution build-up from Monday through Friday, while cities which have better dispersion have more variability during weekdays. We also analyze the correlation of temperatures and NO_2 column amounts and find that NO_2 is larger on the hottest days (>32°C) as compared to warm days (26°C - 32°C), which is in contrast to a general decrease in NO_2 with increasing temperature at lower temperature bins. Finally, we compare column NO_2 with estimates of surface $PM_{2.5}$ and find fairly poor correlation, suggesting that NO_2 and $PM_{2.5}$ are becoming increasingly less correlated in CONUS. These new developments make TROPOMI NO_2 satellite data advantageous for policymakers and public health officials, who request information at high spatial resolution and short timescales, in order to assess, devise, and evaluate regulations.

Introduction

Enhancements of NO_2 serve as a stark reminder of our society's global reliance on fossil-fuel combustion. NO_2 – which comprises ~70% of NO_X (NO_X = NO + NO_2) in urban airsheds (Valin et al., 2013) – primarily originates as a byproduct of fossil-fuel combustion, although there are some biogenic sources of NO_2 such as lightning and microbes in soil (Jacob, 2000). NO_2 is a toxic air pollutant, which can cause and exacerbate asthma in vulnerable populations (Achakulwisut et al., 2019; Anenberg et al., 2018) and lead to premature mortality (Burnett et al., 2004). NO_2 can also react in the atmosphere to create tropospheric ozone (O_3), which is noted for its damaging effects including premature aging of lungs (Broeckaert et al., 1999; McConnell et al., 2002) and premature mortality (Bell, 2004; Bell et al., 2006). HNO_3 often represents the final chemical state of NO_2 in the atmosphere and when deposited, agitates the equilibrium of our ecosystems due to its acidic properties (Burns et al., 2016). NO_2 can also participate in a series of reactions to create particulate nitrate (NO_3^-), a component of fine particulate matter less than 2.5 microns in diameter ($PM_{2.5}$), which is the leading cause of mortality due to air pollution (Cohen et al., 2017).

There is a rich legacy of monitoring NO_2 by remote sensing instruments (Burrows et al., 1999). NO_2 can be observed from space because it has unique high-frequency spectral features within the 400 – 500 nm wavelength region (Vandaele et al., 1998). The newest remote sensing spectrometer, TROPOMI (VanGeffen et al., 2019; Veefkind et al., 2012), has been gathering data on the global heterogeneities of NO_2 air pollution since October 2017. This instrument builds on the legacy of prior Ultraviolet – Visible (UV-Vis) spectrometers including the Global Ozone Monitoring Experiment (GOME) (Burrows et al., 1999; Martin et al., 2002; Richter & Burrows, 2002), the Scanning Imaging Spectrometer for Atmospheric Chartography (SCIAMACHY) (Bovensmann et al., 1999; Heue et al., 2005), the Global Ozone Monitoring Experiment - 2 (GOME-2) instrument (Munro et al., 2016; Richter et al., 2011), and the Ozone Monitoring Instrument (OMI) (Boersma et al., 2018; Krotkov et al., 2017; Levelt et al., 2006, 2018).

Satellite-based remote sensing instruments can be particularly useful in quantifying the trends of NO_X pollution in high-emission areas (Castellanos & Boersma, 2012; Duncan et al., 2016; Georgoulias et al., 2019; Krotkov et al., 2016; McLinden et al., 2016; Stavrakou et al., 2008; Van

Der A et al., 2008), the seasonal cycles of air pollution (Ialongo et al., 2016; Shah et al., 2020), and the weekly cycle of NO_X emissions (Beirle et al., 2003; Ialongo et al., 2016; Ma et al., 2013; Russell et al., 2010; Valin et al., 2014). In an additional step, NO_X emissions can be computed by combining the satellite data with meteorological information (Beirle et al., 2011, 2019; de Foy et al., 2015; Goldberg, Lu, Streets, et al., 2019; Goldberg, Saide, et al., 2019; Lorente et al., 2019; Lu et al., 2015; Valin et al., 2013) or by combining the satellite data with chemical transport models (Canty et al., 2015; Cooper et al., 2017; Qu et al., 2017; Souri et al., 2016). Due to the consistency and robustness of the remotely-sensed NO_2 data record, scientists are beginning to infer information from the NO_2 data about other trace gases such as CO_2 (Goldberg, Lu, Oda, et al., 2019; Konovalov et al., 2016; Reuter et al., 2019), CH_4 (de Gouw et al., 2020), and CO (Lama et al., n.d.), since remotely-sensed measurements of those trace gases are generally less reliable. Therefore, remotely-sensed NO_2 can also be helpful in indirectly estimating greenhouse gas emissions.

TROPOMI's smallest pixel size (3.5×7.2 km^2 at nadir, reduced to 3.5×5.6 km^2 at nadir on August 6, 2019) and enhanced sensitivity are significant improvements when compared to previous satellite instruments (Veefkind et al., 2012). NO_2 is unique due to its relatively short photochemical lifetime which varies from 2-5 h during the summer daytime (Beirle et al., 2011; de Foy et al., 2014; Laughner & Cohen, 2019; Valin et al., 2013) to 12-24 h during winter (Shah et al., 2020). As a result, tropospheric NO_2 concentrations are strongly correlated with local NO_X emissions, which are often anthropogenic in origin.

Initial NO_2 measurements from TROPOMI show the complex spatial heterogeneities of NO_2 pollution with more refined resolution than any instrument before it (Griffin et al., 2019; Ialongo et al., 2020). In particular, the smaller pixel sizes aid researchers in differentiating pollution sources within a single metropolitan area such as isolating signals from airports and individual highways (Judd et al., 2019). These small-scale pixel sizes also show better agreement with the spatial features suggested by ground-based measurements (Ialongo et al., 2020; Judd et al., 2019). In particular, modeling studies have shown that matching the NO_2 column to 10% accuracy requires a spatial resolution of at least 4 km (Valin et al., 2011) – the approximate spatial resolution of TROPOMI. Robust high-spatial resolution estimates are also critical inputs

to those trying to quantify the surface-level NO_2 exposures (Geddes et al., 2016; Lamsal et al., 2008; Larkin et al., 2017).

The improved spatial resolution and instrument sensitivity also allows for shorter temporal averaging ranges (days to months) to gain the similar spatial structure it would normally take >1 year to gather (Beirle et al., 2019; Dix et al., 2020; Goldberg, Lu, Streets, et al., 2019; Lorente et al., 2019). As a result, it is easier to gain insight on the short-term variations of NO_X pollution when using TROPOMI, which can be especially helpful for those trying to quantify intra-annual changes in NO_X emissions (F. Liu et al., 2020).

In this paper, we exploit TROPOMI's small pixel sizes and enhanced instrument sensitivity to analyze spatial and temporal features of NO_X columns in the continental United States on annual, seasonal, weekly, and daily timescales. For example, using only a short temporal range of data, we can now answer such questions as:

- Which location within each U.S. state has the worst NO_2 air pollution?
- How does the NO_X emissions cycle vary by day of the week?
- How does temperature affect column NO_2 amounts?
- What is the relative magnitude of NO_2 compared to $PM_{2.5}$?

While older sensors (e.g., OMI) provided insight into some of these questions, early sensors lacked the same sensitivity and required longer oversampling times. Therefore, answers illuminated by TROPOMI provide a "clarity" that has not been seen before.

Methods

TROPOMI NO_2

TROPOMI was launched by the European Space Agency (ESA) for the European Union's Copernicus Sentinel 5 Precursor (S5p) satellite mission on October 13, 2017. The satellite follows a sun-synchronous, low-earth (825 km) orbit with an equator overpass time of approximately 13:30 local solar time (Veefkind et al., 2012). TROPOMI measures total column amounts of several trace gases in the Ultraviolet-Visible-Near Infrared-Shortwave Infrared spectral regions (VanGeffen et al., 2019). This instrument is characterized as a passive optical satellite sensor due to its reliance on solar UV-Visible radiation to gather measurements. At

nadir, pixel sizes are 3.5 × 7 km^2 (reduced to 3.5 × 5.6 km^2 on August 6, 2019) with little variation in pixel sizes across the 2600 km swath. The instrument observes the swath approximately once every second and orbits the Earth in about 100 minutes, resulting in daily global coverage.

Using a differential optical absorption spectroscopy (DOAS) technique on the radiance measurements in the 405 – 465 nm spectral window, the top-of-atmosphere spectral radiances can be converted into slant column amounts of NO_2 between the sensor and the Earth's surface (van Geffen et al., 2020). In two additional steps, the slant column quantity can be converted into a tropospheric vertical column content. In the first step, the stratospheric portion of the column (the amount above approximately 12 km in altitude) is subtracted either by using a measurement in a remote area or by using a global model estimate. In a second step, the slant tropospheric column is converted to a vertical column using a quantity known as the air mass factor. The air mass factor is the most uncertain quantity in the retrieval algorithm (Lorente et al., 2017), and is a function of the surface reflectance, the NO_2 vertical profile, and scattering in the atmosphere among other factors. Using accurate and high-resolution data (spatially and temporally) as inputs in calculating the air mass factor can significantly reduce the overall errors of the air mass factor (S. Choi et al., 2019; Goldberg et al., 2017; Laughner et al., 2016, 2019; Lin et al., 2015; M. Liu et al., 2019; Russell et al., 2011; Zhao et al., 2020) and thus the tropospheric vertical column content.

Operationally, the TM5-MP model (1 × 1° resolution) is used to provide the NO_2 vertical shape profile and the climatological Lambertian Equivalent Reflectivity (0.5 × 0.5° resolution) (Kleipool et al., 2008) is used to provide the surface reflectivities. The operational air mass factor calculation does not explicitly account for aerosol absorption effects, which are accounted for in the effective cloud radiance fraction. While the operational product does have larger uncertainties in the tropospheric column contents than a product with higher spatial resolution inputs, we limit our analysis to relative trends, which dramatically reduces this uncertainty.

Re-gridding

For our analysis we re-grid the operational TROPOMI tropospheric vertical column NO_2, with native pixels of approximately 3.5 × 7 km^2, to a newly defined 0.01° × 0.01° grid (approximately 1 × 1 km^2) centered over the continental United States (CONUS; corner points: SW: 24.5° N,

124.75° W; NE: 49.5° N, 66.75° W). Before re-gridding, the data are filtered so as to use only the highest quality measurements (quality assurance flag (QA_flag) > 0.75). Once the re-gridding has been completed, the data is averaged over varying timeframes as discussed in the results section.

Other Datasets

Additionally, we use two complementary products in some sections of our analysis. When filtering the data based on temperature, we use the maximum daily hourly 2-meter temperature (T2m-Max) from the ERA5 re-analysis. To downscale the ERA5 re-analysis, which is provided at 0.25° × 0.25°, we spatially interpolate daily T2m-Max to 0.01° × 0.01° using bilinear interpolation. For that reason, the heat-urban island effect and any microscale meteorology features (e.g., sea breezes) will not be accounted for, but these effects should be minor for our particular analysis, which groups temperatures in 5° C intervals. We also compare our 0.01° × 0.01° TROPOMI NO_2 data to an annual $PM_{2.5}$ dataset at the same spatial resolution (VanDonkelaar et al., 2019).

Results

TROPOMI NO_2 in CONUS

Figure 1 depicts the 2019 CONUS annual average of TROPOMI tropospheric vertical column NO_2 compared to averages over shorter timeframes.

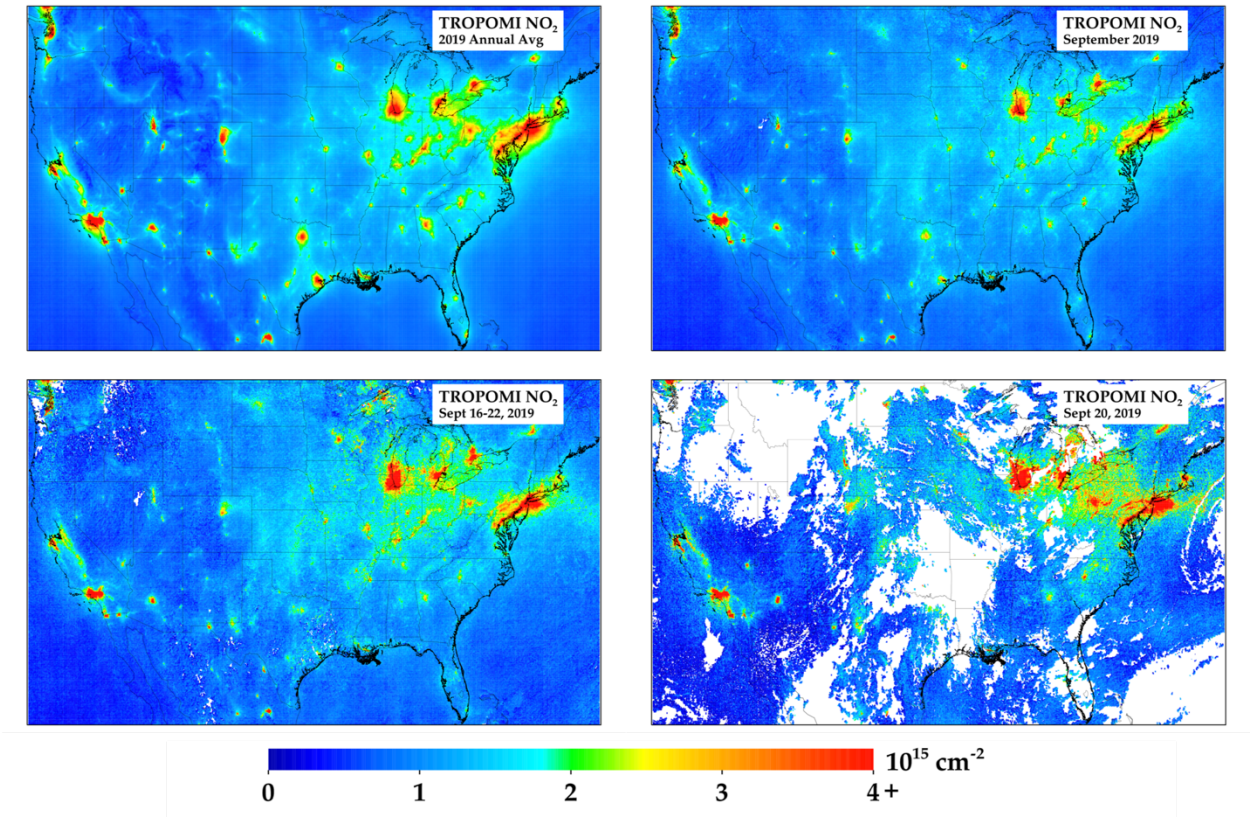

Figure 1. TROPOMI NO_2 oversampled to 0.01° × 0.01° spatial resolution for four different temporal resolutions: (top left) annual, (top right) monthly, (bottom left) weekly, and (bottom right) daily.

This example illustrates how shorter timeframes compare to the annual average in both magnitude and clarity. In the single daily snapshot (September 20, 2019), there are wide sections that are missing due to cloud coverage. In the areas that do have coverage, values can be a factor of five different than the annual average, but the spatial heterogeneities are generally captured. When oversampling over a one-week period (September 16 – 22, 2019), the image quickly starts to resemble the annual average with some differences in magnitude due to meteorological factors, such as temperature (which will be discussed later). The one-week average can therefore be considered the minimum amount of oversampling time to properly capture spatial heterogeneities. A monthly oversampled image essentially captures the same spatial

heterogeneities as the annual average, but with magnitude differences due to meteorology. It should be noted that September was specifically chosen for this analysis due to its propensity to have both less cloud coverage and snow cover than other months. If oversampling during winter months (i.e., Dec – March), which tend to have fewer ideal conditions for satellite retrievals of trace gases, oversampling times will need to be longer to achieve similar clarity.

When visually inspecting the CONUS TROPOMI NO_2 average during the initial twenty months of the TROPOMI record (May 1, 2018 – Dec 31, 2019) (Figure 2), we now start to see clear spatial heterogeneities across the domain. The largest U.S. cities can be seen and their magnitudes can be compared to each other (results further discussed later).

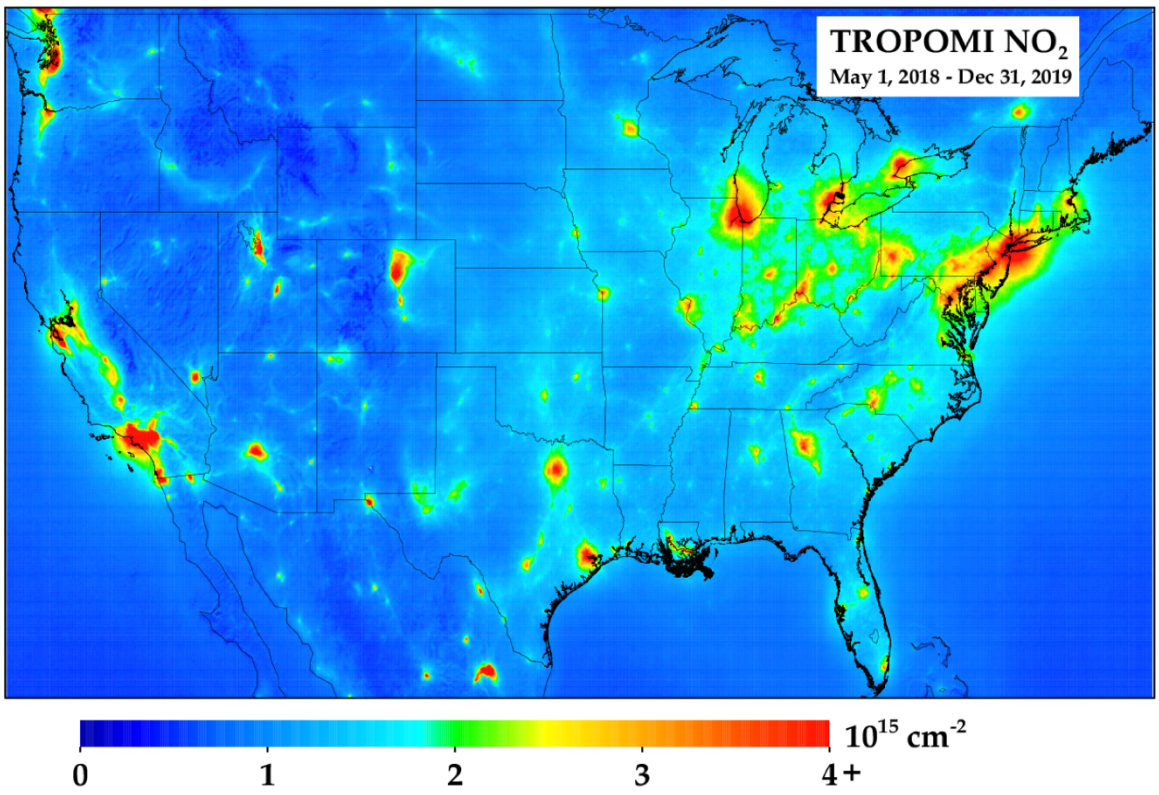

Figure 2. TROPOMI NO_2 oversampled to 0.01° × 0.01° spatial resolution during May 1, 2018 – December 31, 2019. Only pixels exceeding a quality assurance flag of 0.75 are included.

Equally important, smaller sources of NO_2 pollution can now be observed, and they are not spatially smeared into the background NO_2 concentration. For example, when magnifying the western United States (Figure 3), the roadway network and related activity in the Idaho Snake River valley can be clearly observed. Other examples are the copper mining operations in

eastern Arizona associated with the Morenci Mine, the coal mining operations in the Powder River Basin in eastern Wyoming, and to a lesser extent the gold mining operations associated with the Goldstrike mine in Nevada. In addition, NO_2 concentrations are clearly correlated with oil & gas operations in the Permian (Texas) and Bakken (North Dakota) basins (also discussed in (Dix et al., 2020)) and is > 5 times larger than the NO_2 in the rural areas upwind. Individual spikes in NO_2 associated with NO_X emissions from large power plants (e.g., Navajo in Arizona, Craig in Colorado, Colstrip in Montana, North Valmy in Nevada, Four Corners/San Juan in New Mexico, Intermountain, Bonanza, Hunter/Huntington in Utah, Jim Bridger in Wyoming) can also be observed during this 2018-2019 period even though there have been large reductions (~85%) in the NO_X emissions from most of these power plants since the introduction of the federally-mandated NO_X SIP call in 2003.

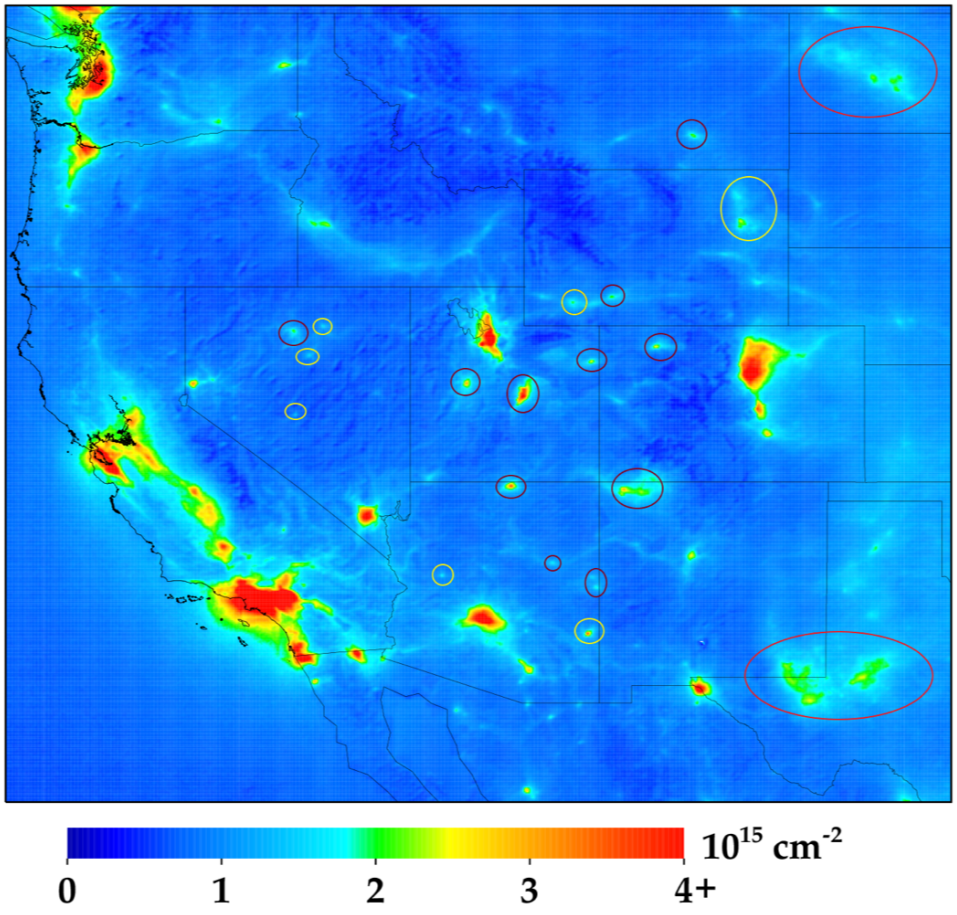

Figure 3. Same data shown in Figure 2, but now zoomed into the western United States. Power plants are outlined in dark magenta, mining operations in yellow, and oil & gas in bright red.

TROPOMI data is especially powerful in analyzing local variations in NO_2 pollution as compared to predecessor instruments. In Figure 4, we zoom into five different U.S. states, and in Table 1 we provide the largest NO_2 values in each state.

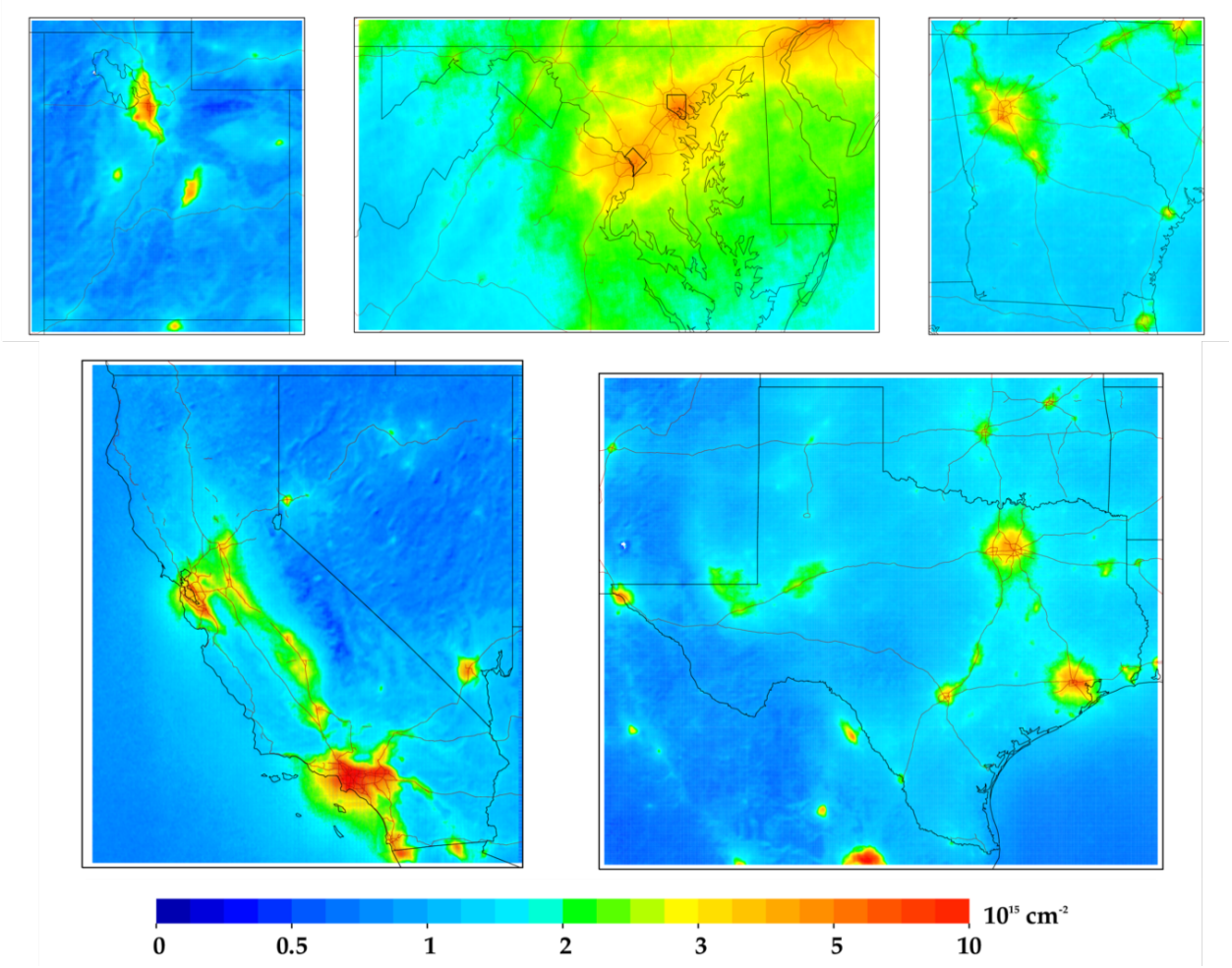

Figure 4. Same data shown in Figure 2, but now zoomed into 5 different U.S. states. Color bar has been adjusted to better differentiate spatial heterogeneities on a local scale.

Table 1. Largest NO_2 column value in each U.S. state during the May 1, 2018 – Dec 31, 2018 period. Ordered by largest to smallest maximum value.

State	Lat	Lon	Value	Detailed location
CA	34.03	-118.18	1.41E+16	E Los Angeles, CA
NY	40.72	-73.97	1.13E+16	East River, Brooklyn, NY
NJ	40.69	-74.14	9.75E+15	Port Newark, NJ
IL	41.82	-87.77	7.31E+15	Cicero, Chicago, IL (near MDW)
WA	47.46	-122.26	6.90E+15	Tukwila, WA (SE Seatle)
IN	41.66	-87.47	6.28E+15	E Chicago, IN (Steel Mill)
UT	40.71	-111.9	6.18E+15	S Salt Lake City, UT
CO	39.76	-105.02	5.98E+15	Highland, Denver, CO
PA	39.95	-75.16	5.95E+15	Downtown Philadelphia, PA
AZ	33.47	-112.15	5.87E+15	Cuatro Palmas, Phoenix, AZ
MI	42.31	-83.11	5.74E+15	Detroit, MI
TX	29.74	-95.14	5.58E+15	Deer Park, Houston, TX
CT	41	-73.67	5.46E+15	Greenwich, CT
NV	36.1	-115.18	4.97E+15	Las Vegas Strip, Las Vegas, NV
MD	39.28	-76.6	4.94E+15	Port of Baltimore, Baltimore, MD
DC	38.89	-77.01	4.65E+15	Capitol Hill, Washington, DC
GA	33.64	-84.42	4.65E+15	Hartsfield Airport, Atlanta, GA
VA	38.88	-77.05	4.59E+15	Pentagon, Arlington, VA
DE	39.8	-75.37	4.34E+15	Claymont, Wilmington, DE
OR	45.52	-122.65	4.25E+15	Buckman, Portland, OR
KY	38.18	-85.73	4.21E+15	Louisville, KY (Airport)
OH	39.12	-84.54	4.20E+15	Cincinatti, OH
MA	42.37	-71.06	4.14E+15	Charlestown, Boston, MA (near BOS)
LA	29.93	-90.14	3.98E+15	Mississippi River, New Orleans, LA
NC	35.24	-80.85	3.76E+15	Catawba, NC (near Marshall Steam SPP)
WV	38.94	-82.11	3.68E+15	Lakin, WV (near Gavin PP)
MO	38.68	-90.19	3.67E+15	Mississippi River, St Louis, MO
KS	39.12	-94.6	3.61E+15	Missouri River, Kansas City, KS
TN	36.16	-86.77	3.52E+15	Nashville, TN
FL	25.85	-80.34	3.40E+15	Medley, Miami, FL
WI	42.86	-87.82	3.40E+15	Oak Creek, WI (near Oak Creek PP)
MN	44.97	-93.24	3.28E+15	Mississippi River, Minneapolis, MN
AL	33.52	-86.82	3.21E+15	Fountain Heights, Birmingham, AL
RI	41.8	-71.41	2.88E+15	S Providence, RI
IA	41.25	-95.88	2.79E+15	Council Bluffs, IA
NE	41.25	-95.88	2.79E+15	Missouri River, Omaha, NE
OK	36.16	-96	2.64E+15	Tulsa, OK
WY	43.69	-105.32	2.52E+15	Thunder Basin Coal, WY
SC	32.88	-79.99	2.52E+15	N Charleston, SC
NM	35.11	-106.62	2.51E+15	Albuquerque, NM
AR	35.12	-90.1	2.46E+15	W Memphis, AR
ID	43.58	-116.23	2.30E+15	Boise, ID (Airport)
ND	47.35	-101.81	2.24E+15	Beulah, ND (near Dakota Gasification Co)
MT	45.86	-106.57	2.20E+15	Colstrip, MT (near Colstrip PP)
NH	42.94	-70.81	1.93E+15	Hampton, NH
ME	43.66	-70.29	1.90E+15	Portland, ME
MS	32.34	-90.19	1.77E+15	Jackson, MS
SD	43.6	-96.74	1.53E+15	N Sioux Falls, SD
VT	42.91	-73.18	1.49E+15	Wilmington, VT

In Figure 5, we zoom into six different U.S. cities. In each instance, the oversampled TROPOMI NO_2 images exhibit features that match known NO_X emissions patterns. The larger NO_2 values correlate very well to the interstate network, population density, and industrial activity hubs (such as manufacturing facilities, airports, and shipping ports). For example, in the image of Maryland, the largest value is observed at the Baltimore Harbor, which is a confluence of several major highways, a large shipping port, the city incinerator, and many industrial facilities. Similarly, the largest values in Chicago exist along the I-55 corridor which has a high traffic volume and a high-density of industrial facilities, with secondary maxima at the O'Hare International airport and the U.S. Steel mill in East Chicago, Indiana. In Los Angeles, the spatial pattern matches the basin outline very well, with the largest values between downtown Los Angeles and Long Beach. In Houston, Texas the largest values are nearest to the petrochemical refining facilities east of town. For all cases, TROPOMI can accurately quantify the relative relationship between the largest sources of NO_X emissions and NO_2 concentrations.

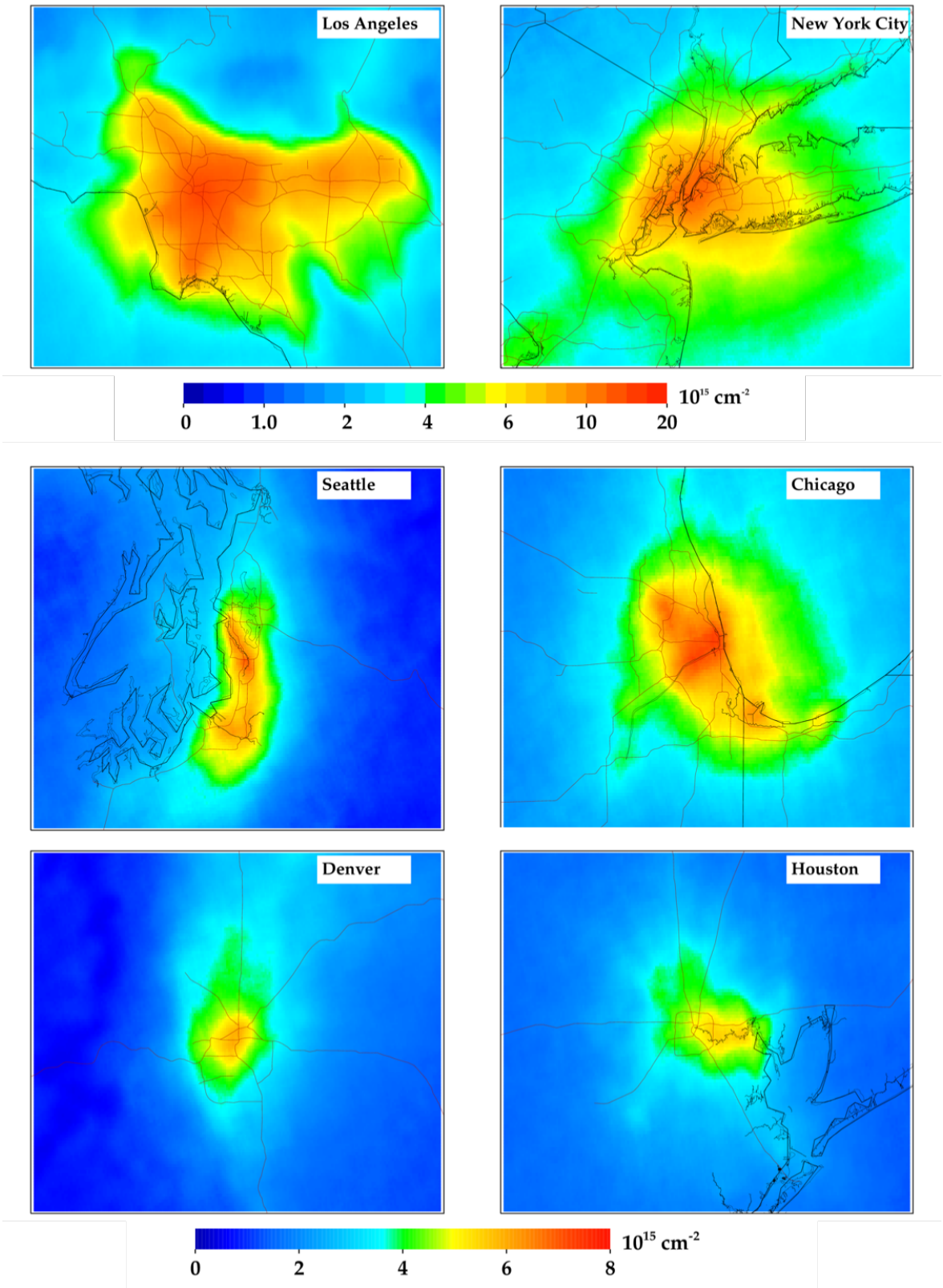

Figure 5. Same data shown in Figure 2, but now zoomed into 6 different U.S. cities. Color bar has been adjusted to better differentiate spatial heterogeneities on a local scale.

Day-of-the-week relationships

A common use of oversampled satellite data is in investigating the weekly cycle of NO_X emissions. In Figure 6, we show the weekly pattern of NO_2 across CONUS for three different days of the week as well as the full weekly cycle in seven U.S. cities. In all cities, the NO_2 appears to be approximately equivalent amongst all weekdays with some minor exceptions. NO_2 pollution is 2.5% larger on Tuesday than a typical weekday, while Mondays and Fridays have 1.4% and 1.3% lower NO_2 pollution than a typical weekday. On Saturdays, NO_2 is 16% lower than the weekday averages, and on Sundays 24% lower.

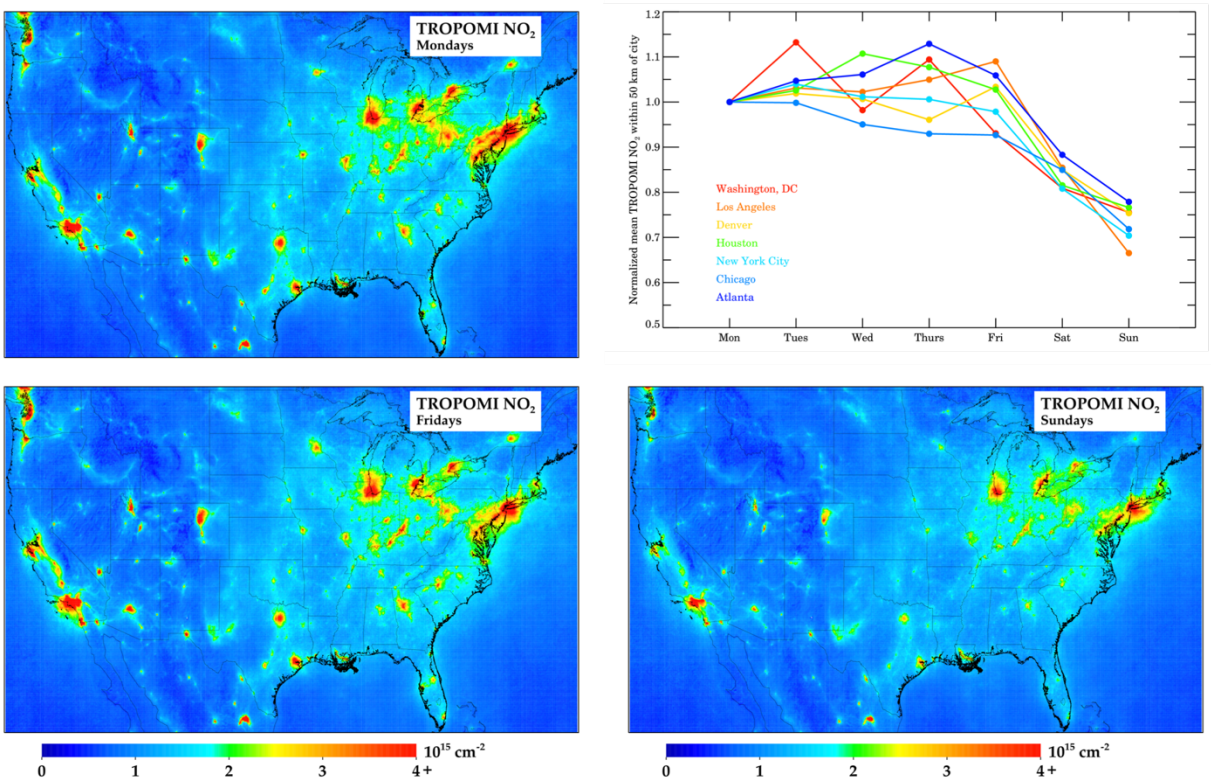

Figure 6. Weekly variations in column NO_2. (Top left) TROPOMI NO_2 during Mondays. (Bottom left) TROPOMI NO_2 during Fridays. (Top right) Weekly variation of TROPOMI NO_2 in 7 U.S. cities normalized to Mondays. (Bottom right) TROPOMI NO_2 during Sundays.

It is interesting to see the differences in the weekday patterns amongst the cities. In Chicago and Washington, D.C., column NO_2 is 10% lower on Fridays compared to earlier days in the week. Conversely, in Los Angeles and Denver, NO_2 is larger on Fridays as compared to previous days of the week. In Chicago and Washington D.C., we hypothesize that this may be an indication of teleworking on Fridays. Conversely, the cities with higher pollution on Fridays, are generally

260 located in mountain valleys with stagnant winds – the valleys may be facilitating an
261 accumulation of pollution during the week.

262 When analyzing the weekday/weekend differences, there should be some consideration for the
263 difference in traffic patterns and general activity between weekends and weekdays. On
264 weekends, traffic counts generally peak in the early afternoon, while on weekdays traffic counts
265 peak in the evening, with a secondary peak in the early morning (de Foy, 2018). Since the
266 satellite observation is acquired in the early afternoon, we suggest that the 24-hour averaged
267 NO_X emissions difference between weekdays and weekends may be even greater than implied by
268 the satellite data. The soon-to-be-launched TEMPO instrument, a geostationary satellite, will
269 hopefully be able to better quantify the morning and evening differences of NO_X emissions
270 (Chance et al., 2019; Penn & Holloway, 2020; Zoogman et al., 2017).

271 **Hot vs. Warm Days**

272 In Figure 7, we show the variation in column NO_2 as a function of the daily maximum 2-meter
273 temperature (T2m-Max). Due to varying climates across the U.S. most cities do not have values
274 for all temperature bins. In general, as temperatures increase, NO_2 decreases; this is primarily
275 driven by $j(NO_2)$ which increases with stronger sunlight. When temperatures are >32°C, we
276 observe a leveling with increasing temperature. This may be related to increasing anthropogenic
277 NO_X emissions (Abel et al., 2017; He et al., 2013) at high temperatures despite a shorter NO_2
278 lifetime. This may also be driven by biogenic or natural causes, such as the faster dissociation of
279 peroxy-acyl nitrates (PANs) or increased soil NO_X emissions (Rasool et al., 2019; Romer et al.,
280 2018) at hot temperatures. The latter reasons are likely causing rural areas to observe increases
281 in NO_2 as temperatures warm above 32°C. The temperature-driven stabilization of NO_2 at very
282 high temperatures appears to hold for all cities except Chicago.

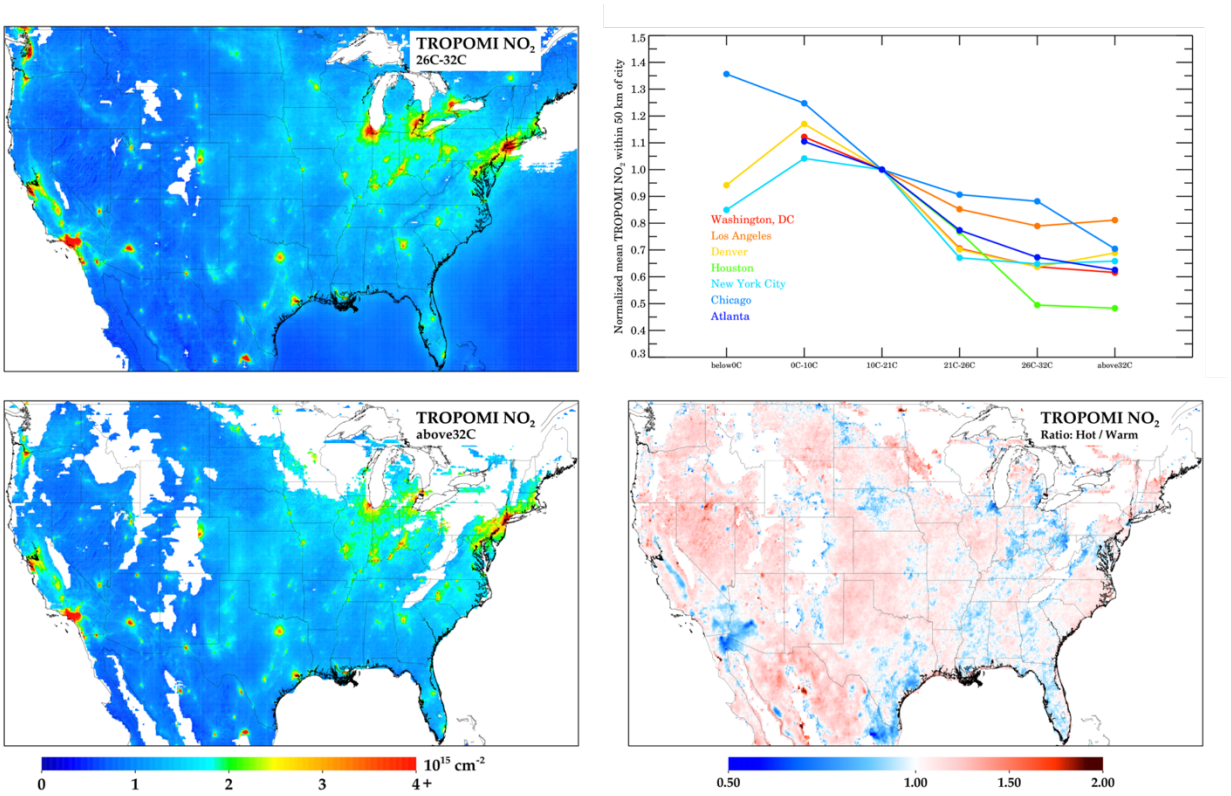

283

284 **Figure 7**. Temperature variations in column NO_2. (Top left) TROPOMI NO_2 when maximum
285 daily 2-m temperature (T2m-Max) is between 26°C – 32°C (Warm; 80°F – 90°F); only areas
286 were >10 valid pixels are shown. (Bottom left) TROPOMI NO_2 when T2m-Max is greater than
287 32°C (Hot; 90°F); only areas were >10 valid pixels are shown. (Top right) Temperature variation
288 of TROPOMI NO_2 in 7 U.S. cities normalized to 10°C – 21°C (50°F – 70°F). (Bottom right)
289 Ratio between bottom left and bottom right panel.

290

291 **Relationship with $PM_{2.5}$**

292 To understand the spatial pattern of NO_2 in comparison to $PM_{2.5}$, we compare TROPOMI annual
293 averages of column NO_2 to estimates of surface-level $PM_{2.5}$ (VanDonkelaar et al., 2019). Both
294 pollutants have generally short atmospheric lifetimes and often have similar regional patterns. In
295 Figure 8, we depict the ratio between normalized TROPOMI NO_2 and normalized surface $PM_{2.5}$
296 using the equation below.

297 $$\frac{PM_{2.5}/\overline{PM_{2.5}}}{NO_2/\overline{NO_2}}$$

298 The red color in Figure 8 indicates that $PM_{2.5}$ is relatively larger than NO_2 and blue indicates that
299 NO_2 is relatively larger than $PM_{2.5}$. There are instances, especially in cities, where $PM_{2.5}$ and

NO_2 are both greater than the CONUS mean, but that one pollutant is much larger than the mean and the other value is only slightly larger than the mean.

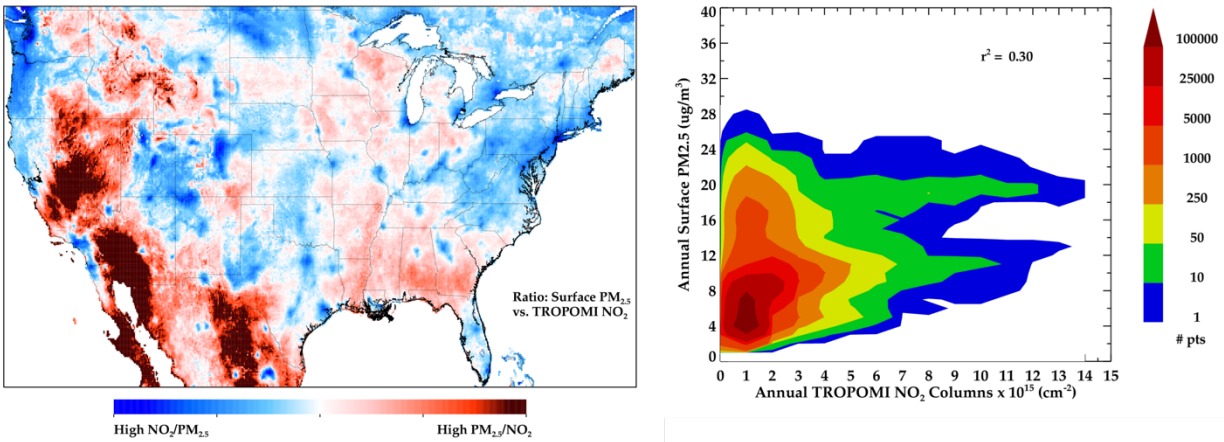

Figure 8. (Left) Ratio of oversampled 2019 TROPOMI NO_2 / 2016 Surface $PM_{2.5}$. (Right) Scatterplot of the two datasets. 2016 is latest year of the 0.01° × 0.01° $PM_{2.5}$ dataset (van Donkelaar et al., 2019) and is used for illustrative purposes. Spatial heterogeneities of annual $PM_{2.5}$ is likely similar between 2016 and 2019.

In major cities (e.g., New York City, Chicago, Los Angeles), NO_2 is more elevated from the mean CONUS concentration compared to $PM_{2.5}$. This is also true regionally in the Northeast and Pacific Northwest. Conversely, $PM_{2.5}$ is relatively elevated compared to the mean in four distinct rural CONUS regions: the desert Southwest, the Intermountain West, the Central Plains, and the Southeast. In the Southwest this is driven by dust. In the Intermountain West, this is likely driven by wildfires. In the Southeast and Central Plains, it is most likely driven by a combination of biogenic aerosols (e.g., secondary organic aerosols) and agricultural operations.

We then compare the NO_2 and $PM_{2.5}$ datasets using a scatterplot. We find low correlation between column NO_2 and surface $PM_{2.5}$ ($r^2 = 0.30$). At high TROPOMI NO_2 values, $PM_{2.5}$ is moderately elevated, but at low TROPOMI NO_2 values, there is a range of distribution of $PM_{2.5}$ with no correlation. This is in general agreement with studies showing that NO_2 hotspots are dominated by local and regional components, while $PM_{2.5}$ is dominated by regional and long-range components, with a lesser influence of local sources (Wang et al., 2020). Nevertheless, we find it important to demonstrate that TROPOMI NO_2 does not appear to be helpful in predicting surface $PM_{2.5}$ in the US.

Conclusions

This study investigates the capabilities of the Tropospheric Monitoring Instrument (TROPOMI) in observing the spatial and temporal patterns of NO_2 pollution in the Continental United States (CONUS). Here, we demonstrate that TROPOMI can capture fine-scale spatial heterogeneities in urban areas, such as hotspots related to airport/shipping operations and high traffic areas; this type of spatial precision cannot be matched by predecessor satellite instruments over short timescales (<1 year). We find that Saturday and Sunday concentrations are 16% and 24% lower respectively than during weekdays, with the caveat that diurnal emissions patterns vary among weekdays and weekends. We also analyze the effects of hot temperatures (>32°C) on NO_2 column amounts and find that column NO_2 is generally larger on the hottest days as compared to warm days (26°C - 32°C). Finally, we compare column NO_2 with estimates of surface $PM_{2.5}$ and find fairly poor correlation, suggesting that NO_2 and $PM_{2.5}$ are not well correlated in CONUS.

For this work, we rely on the operational TROPOMI NO_2 algorithm, which underestimates tropospheric vertical column NO_2 in urban areas. Previous studies suggest that this underestimate is due to the air mass factor (AMF) and ~5km pixel size which cannot resolve street-level variations in concentrations (Goldberg, Lu, Streets, et al., 2019; Griffin et al., 2019; Judd et al., 2019, 2020; Zhao et al., 2020); investigating the effects of the AMF bias on trends as well as investigating the effects of the pixels sizes will be the subject of future work. Also, there may be a clear-sky bias (Geddes et al., 2012) associated with any satellite retrieval, but the general spatial heterogeneities of NO_2 pollution, should be similar amongst all types of weather conditions, when averaged over long timeframes. Lastly, interpreting results from polar-orbiting satellite instruments such as TROPOMI, should be made with some caution due to the mid-day only data collection time. Work quantifying this bias has shown that NO_2 column measurements are lower and incrementally more spatially homogeneous in the afternoon than during the morning (Chong et al., 2018; Fishman et al., 2008; Herman et al., 2019; Knepp et al., 2015; Penn & Holloway, 2020; Tzortziou et al., 2015); it is likely that data from geostationary platforms such as TEMPO (Zoogman et al., 2017), GEMS (W. J. Choi, 2018), and Sentinel 4 (Timmermans et al., 2019), will be able to provide further insight on this time-of-day bias.

Because TROPOMI can observe and measure NO_2 increases attributed to relatively small sources, future work should be able to quantify emissions from small sources (e.g., industrial

activities, small wildfires) that had previously gone undetected from predecessor space-based instruments. Furthermore, due to the instrument's excellent stability, precision, and spatial resolution, it is no longer necessary to average over 6+ months of data to gain a clear depiction of regional NO_2 abundances; instead monthly, weekly or even daily aggregations could suffice for many purposes. The examples presented here demonstrate how TROPOMI NO_2 satellite data can be advantageous for policymakers requesting information at high spatial resolution and short timescales, in order to assess, devise, and evaluate regulations. Future health impact assessment studies can use the high-spatial resolution capabilities of TROPOMI NO_2 to investigate disparities in traffic-related air pollution exposure and associated health effects between neighborhoods and population sub-groups within cities.

Acknowledgments

This work has been supported by the Department of Energy, Office of Fossil Energy. This work has also been sponsored by a Health and Air Quality (HAQ) grant (award #: 80NSSC19K0193), and two Atmospheric Composition Modeling and Analysis Program grants. We would also like to acknowledge valuable comments during the manuscript preparation from Joel Dreessen of Maryland Department of the Environment. TROPOMI NO_2 data can be freely downloaded from the European Space Agency Copernicus Open Access Hub or the NASA EarthData Portal (http://doi.org/10.5270/S5P-s4ljg54). ERA5 can be freely downloaded from the Copernicus Climate Change (C3S) climate data store (CDS) (https://cds.climate.copernicus.eu/#!/search?text=ERA5&type=dataset). The submitted manuscript has been created by UChicago Argonne, LLC, Operator of Argonne National Laboratory ("Argonne"). Argonne, a US Department of Energy Office of Science laboratory, is operated under contract no. DE-AC02-06CH11357.

References

Abel, D. W., Holloway, T., Kladar, R. M., Meier, P., Ahl, D., Harkey, M., & Patz, J. (2017). Response of Power Plant Emissions to Ambient Temperature in the Eastern United States. *Environmental Science and Technology*, *51*(10), 5838–5846. https://doi.org/10.1021/acs.est.6b06201

Achakulwisut, P., Brauer, M., Hystad, P., & Anenberg, S. C. (2019). Global, national, and urban burdens of paediatric asthma incidence attributable to ambient NO_2 pollution: estimates from global datasets. *Lancet Planet Health*. https://doi.org/10.1016/S2542-5196(19)30046-4

Anenberg, S. C., Henze, D. K., Tinney, V., Kinney, P. L., Raich, W., Fann, N., et al. (2018). Estimates of the Global Burden of Ambient PM2.5, Ozone, and NO2 on Asthma Incidence and Emergency Room Visits. *Environmental Health Perspectives*, *126*(10), 107004. https://doi.org/10.1289/EHP3766

Beirle, S., Platt, U., Wenig, M., & Wagner, T. (2003). Weekly cycle of NO2 by GOME measurements: A signature of anthropogenic sources. *Atmospheric Chemistry and Physics*, *3*(6), 2225–2232. https://doi.org/10.5194/acp-3-2225-2003

Beirle, S., Boersma, K. F., Platt, U., Lawrence, M. G., & Wagner, T. (2011). Megacity Emissions and Lifetimes of Nitrogen Oxides Probed from Space. *Science*, *333*(6050), 1737–1739. https://doi.org/10.1126/science.1207824

Beirle, S., Borger, C., Dörner, S., Li, A., Hu, Z., Liu, F., et al. (2019). Pinpointing nitrogen oxide emissions from space. *Science Advances*, *5*(11), eaax9800. https://doi.org/10.1126/sciadv.aax9800

Bell, M. L. (2004). Ozone and Short-term Mortality in 95 US Urban Communities, 1987-2000. *Jama*, *292*(19), 2372. https://doi.org/10.1001/jama.292.19.2372

Bell, M. L., Peng, R. D., & Dominici, F. (2006). The exposure-response curve for ozone and risk of mortality and the adequacy of current ozone regulations. *Environmental Health Perspectives*, *114*(4), 532–536. https://doi.org/10.1289/ehp.8816

Boersma, K. F., Eskes, H. J., Richter, A., De Smedt, I., Lorente, A., Beirle, S., et al. (2018). Improving algorithms and uncertainty estimates for satellite NO2 retrievals: results from the quality assurance for the essential climate variables (QA4ECV) project. *Atmospheric Measurement Techniques*, *11*(12), 6651–6678. https://doi.org/10.5194/amt-11-6651-2018

Bovensmann, H., Burrows, J. P., Buchwitz, M., Frerick, J., Noël, S., Rozanov, V. V., et al. (1999). SCIAMACHY: Mission Objectives and Measurement Modes. *Journal of the Atmospheric Sciences*, *56*(2), 127–150. https://doi.org/10.1175/1520-0469(1999)056<0127:SMOAMM>2.0.CO;2

Broeckaert, F., Arsalane, K., Hermans, C., Bergamaschi, E., Brustolin, A., Mutti, A., & Bernard, A. (1999). Lung epithelial damage at low concentrations of ambient ozone. *Lancet*, *353*(9156), 900–901. https://doi.org/10.1016/S0140-6736(99)00540-1

Burnett, R. T., Stieb, D., Brook, J. R., Cakmak, S., Dales, R., Raizenne, M., et al. (2004). Associations between short-term changes in nitrogen dioxide and mortality in Canadian

cities. *Archives of Environmental Health*, *59*(5), 228–236. https://doi.org/10.3200/AEOH.59.5.228-236

Burns, D. A., Gay, D. A., & Lehmann, C. M. B. (2016). Acid rain and its environmental effects: Recent scientific advances. *Atmospheric Environment*, *146*, 1–4. https://doi.org/10.1016/J.ATMOSENV.2016.10.019

Burrows, J. P., Weber, M., Buchwitz, M., Rozanov, V., Ladstatter-Weibenmayer, A., Richter, A., et al. (1999). The Global Ozone Monitoring Experiment (GOME): Mission Concept and First Scientific Results. *Journal of Atmospheric Sciences*, *56*, 151–175. https://doi.org/10.1175/1520-0469(1999)056<0151:TGOMEG>2.0.CO;2

Canty, T. P., Hembeck, L., Vinciguerra, T. P., Anderson, D. C., Goldberg, D. L., Carpenter, S. F., et al. (2015). Ozone and NO<inf>x</inf> chemistry in the eastern US: Evaluation of CMAQ/CB05 with satellite (OMI) data. *Atmospheric Chemistry and Physics*, *15*(19), 10965–10982. https://doi.org/10.5194/acp-15-10965-2015

Castellanos, P., & Boersma, K. F. (2012). Reductions in nitrogen oxides over Europe driven by environmental policy and economic recession. *Scientific Reports*, *2*(2), 1–7. https://doi.org/10.1038/srep00265

Chance, K., Liu, X., Miller, C. C., González Abad, G., Huang, G., Nowlan, C., et al. (2019). TEMPO Green Paper: Chemistry, physics, and meteorology experiments with the Tropospheric Emissions: monitoring of pollution instrument. In S. P. Neeck, T. Kimura, & P. Martimort (Eds.), *Sensors, Systems, and Next-Generation Satellites XXIII* (Vol. 11151, p. 10). SPIE. https://doi.org/10.1117/12.2534883

Choi, S., Lamsal, L. N., Follette-Cook, M., Joiner, J., Krotkov, N. A., Swartz, W. H., et al. (2019). Assessment of NO2 observations during DISCOVER-AQ and KORUS-AQ field campaigns. *AMTD*. https://doi.org/10.5194/amt-2019-338

Choi, W. J. (2018). Introducing the geostationary environment monitoring spectrometer. *Journal of Applied Remote Sensing*, *12*(04), 1. https://doi.org/10.1117/1.JRS.12.044005

Chong, H., Lee, H., Koo, J. H., Kim, J., Jeong, U., Kim, W., et al. (2018). Regional characteristics of NO2 column densities from pandora observations during the MAPS-Seoul campaign. *Aerosol and Air Quality Research*, *18*(9), 2207–2219. https://doi.org/10.4209/aaqr.2017.09.0341

Cohen, A. J., Brauer, M., Burnett, R. T., Anderson, H. R., Frostad, J., Estep, K., et al. (2017). Estimates and 25-year trends of the global burden of disease attributable to ambient air pollution: an analysis of data from the Global Burden of Diseases Study 2015. *The Lancet*, *389*(10082), 1907–1918. https://doi.org/10.1016/S0140-6736(17)30505-6

Cooper, M. J., Martin, R. V., Padmanabhan, A., & Henze, D. K. (2017). Comparing mass balance and adjoint methods for inverse modeling of nitrogen dioxide columns for global nitrogen oxide emissions. *Journal of Geophysical Research*, *122*(8), 4718–4734. https://doi.org/10.1002/2016JD025985

Dix, B., Bruin, J., Roosenbrand, E., Vlemmix, T., Francoeur, C., Gorchov-Negron, A., et al. (2020). Nitrogen Oxide Emissions from U.S. Oil and Gas Production: Recent Trends and

Source Attribution. *Geophysical Research Letters*, *47*(1), 2019GL085866. https://doi.org/10.1029/2019GL085866

Duncan, B. N., Lamsal, L. N., Thompson, A. M., Yoshida, Y., Lu, Z., Streets, D. G., et al. (2016). A space-based, high-resolution view of notable changes in urban NOx pollution around the world (2005-2014). *Journal of Geophysical Research: Atmospheres*, *121*(2), 976–996. https://doi.org/10.1002/2015JD024121

Fishman, J., Bowman, K. W., Burrows, J. P., Richter, A., Chance, K. V., Edwards, D. P., et al. (2008). Remote Sensing of Tropospheric Pollution from Space. *Bulletin of the American Meteorological Society*, *89*(6), 805–822. https://doi.org/10.1175/2008BAMS2526.1

de Foy, B. (2018). City-level variations in NOx emissions derived from hourly monitoring data in Chicago. *Atmospheric Environment*, *176*(x), 128–139. https://doi.org/10.1016/j.atmosenv.2017.12.028

de Foy, B., Wilkins, J. L., Lu, Z., Streets, D. G., & Duncan, B. N. (2014). Model evaluation of methods for estimating surface emissions and chemical lifetimes from satellite data. *Atmospheric Environment*, *98*, 66–77. https://doi.org/10.1016/j.atmosenv.2014.08.051

de Foy, B., Lu, Z., Streets, D. G., Lamsal, L. N., & Duncan, B. N. (2015). Estimates of power plant NOx emissions and lifetimes from OMI NO2 satellite retrievals. *Atmospheric Environment*, *116*(2), 1–11. https://doi.org/10.1016/j.atmosenv.2015.05.056

Geddes, J. A., Murphy, J. G., O'Brien, J. M., & Celarier, E. A. (2012). Biases in long-term NO2 averages inferred from satellite observations due to cloud selection criteria. *Remote Sensing of Environment*, *124*(2), 210–216. https://doi.org/10.1016/j.rse.2012.05.008

Geddes, J. A., Martin, R. V., Boys, B. L., & van Donkelaar, A. (2016). Long-Term Trends Worldwide in Ambient NO 2 Concentrations Inferred from Satellite Observations. *Environmental Health Perspectives*, *124*(3), 281–289. https://doi.org/10.1289/ehp.1409567

van Geffen, J., Boersma, K. F., Eskes, H., Sneep, M., ter Linden, M., Zara, M., & Veefkind, J. P. (2020). S5P TROPOMI NO₂ slant column retrieval: method, stability, uncertainties and comparisons with OMI. *Atmospheric Measurement Techniques*, *13*(3), 1315–1335. https://doi.org/10.5194/amt-13-1315-2020

Georgoulias, A. K., van der A, R. J., Stammes, P., Boersma, K. F., & Eskes, H. J. (2019). Trends and trend reversal detection in 2 decades of tropospheric NO2 satellite observations. *Atmospheric Chemistry and Physics*, *19*(9), 6269–6294. https://doi.org/10.5194/acp-19-6269-2019

Goldberg, D. L., Lamsal, L. N., Loughner, C. P., Swartz, W. H., Lu, Z., & Streets, D. G. (2017). A high-resolution and observationally constrained OMI NO2 satellite retrieval. *Atmospheric Chemistry and Physics*, *17*(18), 11403–11421. https://doi.org/10.5194/acp-17-11403-2017

Goldberg, D. L., Saide, P. E., Lamsal, L. N., de Foy, B., Lu, Z., Woo, J.-H., et al. (2019). A top-down assessment using OMI NO2 suggests an underestimate in the NOx emissions inventory in Seoul, South Korea, during KORUS-AQ. *Atmospheric Chemistry and Physics*, *19*(3), 1801–1818. https://doi.org/10.5194/acp-19-1801-2019

Goldberg, D. L., Lu, Z., Streets, D. G., de Foy, B., Griffin, D., McLinden, C. A., et al. (2019).

Enhanced Capabilities of TROPOMI NO2 : Estimating NOx from North American Cities and Power Plants. *Environmental Science & Technology*, acs.est.9b04488. https://doi.org/10.1021/acs.est.9b04488

Goldberg, D. L., Lu, Z., Oda, T., Lamsal, L. N., Liu, F., Griffin, D., et al. (2019). Exploiting OMI NO2 satellite observations to infer fossil-fuel CO2 emissions from U.S. megacities. *Science of The Total Environment*, *695*, 133805. https://doi.org/10.1016/j.scitotenv.2019.133805

de Gouw, J. A., Veefkind, J. P., Roosenbrand, E., Dix, B., Lin, J. C., Landgraf, J., & Levelt, P. F. (2020). Daily Satellite Observations of Methane from Oil and Gas Production Regions in the United States. *Scientific Reports*, *10*(1), 1379. https://doi.org/10.1038/s41598-020-57678-4

Griffin, D., Zhao, X., McLinden, C. A., Boersma, K. F., Bourassa, A., Dammers, E., et al. (2019). High-Resolution Mapping of Nitrogen Dioxide With TROPOMI: First Results and Validation Over the Canadian Oil Sands. *Geophysical Research Letters*, *46*(2), 1049–1060. https://doi.org/10.1029/2018GL081095

He, H., Hembeck, L., Hosley, K. M., Canty, T. P., Salawitch, R. J., & Dickerson, R. R. (2013). High ozone concentrations on hot days: The role of electric power demand and NOx emissions. *Geophysical Research Letters*, *40*(19), 5291–5294. https://doi.org/10.1002/grl.50967

Herman, J., Abuhassan, N., Kim, J., Kim, J., Dubey, M., Raponi, M., & Tzortziou, M. (2019). Underestimation of column NO2 amounts from the OMI satellite compared to diurnally varying ground-based retrievals from multiple PANDORA spectrometer instruments. *Atmospheric Measurement Techniques*, *12*(10), 5593–5612. https://doi.org/10.5194/amt-12-5593-2019

Heue, K.-P., Richter, A., Bruns, M., Burrows, J. P., Friedeburg, C. V, Platt, U., et al. (2005). Validation of SCIAMACHY tropospheric NO2 columns with AMAXDOAS measurements. *Atmospheric Chemistry and Physics*, *5*, 1039–1051. Retrieved from www.atmos-chem-phys.org/acp/5/1039/SRef-ID:1680-7324/acp/2005-5-1039EuropeanGeosciencesUnion

Ialongo, I., Herman, J. R., Krotkov, N., Lamsal, L. N., Folkert Boersma, K., Hovila, J., & Tamminen, J. (2016). Comparison of OMI NO2 observations and their seasonal and weekly cycles with ground-based measurements in Helsinki. *Atmospheric Measurement Techniques*, *9*(10), 5203–5212. https://doi.org/10.5194/amt-9-5203-2016

Ialongo, I., Virta, H., Eskes, H., Hovila, J., & Douros, J. (2020). Comparison of TROPOMI/Sentinel-5 Precursor NO2 observations with ground-based measurements in Helsinki. *Atmospheric Measurement Techniques*, *13*(1), 205–218. https://doi.org/10.5194/amt-13-205-2020

Jacob, D. J. (2000). Heterogeneous chemistry and tropospheric ozone. *Atmospheric Environment*, *34*(12–14), 2131–2159. https://doi.org/10.1016/S1352-2310(99)00462-8

Judd, L. M., Al-Saadi, J. A., Janz, S. J., Kowalewski, M. G., Pierce, R. B., Szykman, J. J., et al. (2019). Evaluating the impact of spatial resolution on tropospheric NO2 column comparisons within urban areas using high-resolution airborne data. *Atmos. Meas. Tech*, *12*,

6091–6111. https://doi.org/10.5194/amt-12-6091-2019

Judd, L. M., Al-Saadi, J. A., Szykman, J. J., Valin, L. C., Janz, S. J., Kowalewski, M. G., et al. (2020). Evaluating Sentinel-5P TROPOMI tropospheric NO2 column densities with airborne and Pandora spectrometers near New York City and Long Island Sound. *AMTD*. https://doi.org/10.5194/amt-2020-151

Kleipool, Q. L., Dobber, M. R., de Haan, J. F., & Levelt, P. F. (2008). Earth surface reflectance climatology from 3 years of OMI data. *Journal of Geophysical Research Atmospheres*, *113*(18), 1–22. https://doi.org/10.1029/2008JD010290

Knepp, T., Pippin, M., Crawford, J., Chen, G., Szykman, J., Long, R. W., et al. (2015). Estimating surface NO2 and SO2 mixing ratios from fast-response total column observations and potential application to geostationary missions. *Journal of Atmospheric Chemistry*, *72*(3–4), 261–286. https://doi.org/10.1007/s10874-013-9257-6

Konovalov, I. B., Berezin, E. V., Ciais, P., Broquet, G., Zhuravlev, R. V., & Janssens-Maenhout, G. (2016). Estimation of fossil-fuel CO2 emissions using satellite measurements of "proxy" species. *Atmospheric Chemistry and Physics*, *16*(21), 13509–13540. https://doi.org/10.5194/acp-16-13509-2016

Krotkov, N. A., McLinden, C. A., Li, C., Lamsal, L. N., Celarier, E. A., Marchenko, S. V., et al. (2016). Aura OMI observations of regional SO2 and NO2 pollution changes from 2005 to 2015. *Atmospheric Chemistry and Physics*, *16*(7), 4605–4629. https://doi.org/10.5194/acp-16-4605-2016

Krotkov, N. A., Lamsal, L. N., Celarier, E. A., Swartz, W. H., Marchenko, S. V., Bucsela, E. J., et al. (2017). The version 3 OMI NO2standard product. *Atmospheric Measurement Techniques*, *10*(9), 3133–3149. https://doi.org/10.5194/amt-10-3133-2017

Lama, S., Houweling, S., Folkert Boersma, K., Aben, I., Denier Van Der Gon, H. A. C., Krol, M. C., et al. (n.d.). Quantifying burning efficiency in Megacities using NO 2 /CO ratio from the Tropospheric Monitoring Instrument (TROPOMI). *ACPD*. https://doi.org/10.5194/acp-2019-1112

Lamsal, L. N., Martin, R. V., van Donkelaar, A., Steinbacher, M., Celarier, E. A., Bucsela, E., et al. (2008). Ground-level nitrogen dioxide concentrations inferred from the satellite-borne Ozone Monitoring Instrument. *Journal of Geophysical Research Atmospheres*, *113*(16), 1–15. https://doi.org/10.1029/2007JD009235

Larkin, A., Geddes, J. A., Martin, R. V., Xiao, Q., Liu, Y., Marshall, J. D., et al. (2017). Global Land Use Regression Model for Nitrogen Dioxide Air Pollution. *Environmental Science and Technology*, *51*(12), 6957–6964. https://doi.org/10.1021/acs.est.7b01148

Laughner, J. L., & Cohen, R. C. (2019). Direct observation of changing NOx lifetime in North American cities. *Science*, *366*(6466), 723–727. https://doi.org/10.1126/science.aax6832

Laughner, J. L., Zare, A., & Cohen, R. C. (2016). Effects of daily meteorology on the interpretation of space-based remote sensing of NO2. *Atmospheric Chemistry and Physics*, *16*(23), 15247–15264. https://doi.org/10.5194/acp-16-15247-2016

Laughner, J. L., Zhu, Q., & Cohen, R. C. (2019). Evaluation of version 3.0B of the BEHR OMI

NO2 product. *Atmospheric Measurement Techniques*, *12*(1), 129–146. https://doi.org/10.5194/amt-12-129-2019

Levelt, P. F., Oord, G. H. J. Van Den, Dobber, M. R., Dirksen, R. J., MÄLKKI, A., VISSER, H., et al. (2006). The ozone monitoring instrument. *Ieee Transactions on Geoscience and Remote Sensing*, *44*(5), 1093–1101. https://doi.org/Urn:nbn:nl:ui:25-648485

Levelt, P. F., Joiner, J., Tamminen, J., Veefkind, J. P., Bhartia, P. K., Zweers, D. C. S., et al. (2018). The Ozone Monitoring Instrument: Overview of 14 years in space. *Atmospheric Chemistry and Physics*, *18*(8), 5699–5745. https://doi.org/10.5194/acp-18-5699-2018

Lin, J. T., Liu, M. Y., Xin, J. Y., Boersma, K. F., Spurr, R., Martin, R. V., & Zhang, Q. (2015). Influence of aerosols and surface reflectance on satellite NO2 retrieval: Seasonal and spatial characteristics and implications for NOx emission constraints. *Atmospheric Chemistry and Physics*, *15*(19), 11217–11241. https://doi.org/10.5194/acp-15-11217-2015

Liu, F., Page, A., Strode, S. A., Yoshida, Y., Choi, S., Zheng, B., et al. (2020). Abrupt declines in tropospheric nitrogen dioxide over China after the outbreak of COVID-19. Retrieved from http://arxiv.org/abs/2004.06542

Liu, M., Lin, J., Boersma, K. F., Pinardi, G., Wang, Y., Chimot, J., et al. (2019). Improved aerosol correction for OMI tropospheric NO2 retrieval over East Asia: constraint from CALIOP aerosol vertical profile. *Atmospheric Measurement Techniques*, *12*(1), 1–21. https://doi.org/10.5194/amt-12-1-2019

Lorente, A., Folkert Boersma, K., Yu, H., Dörner, S., Hilboll, A., Richter, A., et al. (2017). Structural uncertainty in air mass factor calculation for NO2 and HCHO satellite retrievals. *Atmospheric Measurement Techniques*, *10*(3), 759–782. https://doi.org/10.5194/amt-10-759-2017

Lorente, A., Boersma, K. F., Eskes, H. J., Veefkind, J. P., van Geffen, J. H. G. M., de Zeeuw, M. B., et al. (2019). Quantification of nitrogen oxides emissions from build-up of pollution over Paris with TROPOMI. *Scientific Reports*, *9*(1), 20033. https://doi.org/10.1038/s41598-019-56428-5

Lu, Z., Streets, D. G., de Foy, B., Lamsal, L. N., Duncan, B. N., & Xing, J. (2015). Emissions of nitrogen oxides from US urban areas: Estimation from Ozone Monitoring Instrument retrievals for 2005-2014. *Atmospheric Chemistry and Physics*, *15*(18), 10367–10383. https://doi.org/10.5194/acp-15-10367-2015

Ma, J. Z., Beirle, S., Jin, J. L., Shaiganfar, R., Yan, P., & Wagner, T. (2013). Tropospheric NO2 vertical column densities over Beijing: Results of the first three years of ground-based MAX-DOAS measurements (2008-2011) and satellite validation. *Atmospheric Chemistry and Physics*, *13*(3), 1547–1567. https://doi.org/10.5194/acp-13-1547-2013

Martin, R. V., Chance, K., Jacob, D. J., Kurosu, T. P., Spurr, R. J. D., Bucsela, E., et al. (2002). An improved retrieval of tropospheric nitrogen dioxide from GOME. *Journal of Geophysical Research D: Atmospheres*, *107*(20). https://doi.org/10.1029/2001JD001027

McConnell, R., Berhane, K., Gilliland, F., London, S. J., Islam, T., Gauderman, W. J., et al. (2002). Asthma in exercising children exposed to ozone: a cohort study. *Lancet (London,*

616 *England)*, *359*(9304), 386–91. https://doi.org/10.1016/S0140-6736(02)07597-9

617 McLinden, C. A., Fioletov, V. E., Krotkov, N. A., Li, C., Boersma, K. F., & Adams, C. (2016).
618 A Decade of Change in NO2 and SO2 over the Canadian Oil Sands As Seen from Space.
619 *Environmental Science and Technology*, *50*(1), 331–337.
620 https://doi.org/10.1021/acs.est.5b04985

621 Munro, R., Lang, R., Klaes, D., Poli, G., Retscher, C., Lindstrot, R., et al. (2016). The GOME-2
622 instrument on the Metop series of satellites: instrument design, calibration, and level 1 data
623 processing – an overview. *Atmospheric Measurement Techniques*, *9*(3), 1279–1301.
624 https://doi.org/10.5194/amt-9-1279-2016

625 Penn, E., & Holloway, T. (2020). Evaluating current satellite capability to observe diurnal
626 change in nitrogen oxides in preparation for geostationary satellite missions. *Environmental*
627 *Research Letters*. https://doi.org/10.1088/1748-9326/ab6b36

628 Qu, Z., Henze, D. K., Capps, S. L., Wang, Y., Xu, X., Wang, J., & Keller, M. (2017). Monthly
629 top-down NOxemissions for China (2005-2012): A hybrid inversion method and trend
630 analysis. *Journal of Geophysical Research*, *122*(8), 4600–4625.
631 https://doi.org/10.1002/2016JD025852

632 Rasool, Q. Z., Bash, J. O., & Cohan, D. S. (2019). Mechanistic representation of soil nitrogen
633 emissions in the Community Multiscale Air Quality (CMAQ) model v 5.1. *Geosci. Model*
634 *Dev*, *12*, 849–878. https://doi.org/10.5194/gmd-12-849-2019

635 Reuter, M., Buchwitz, M., Schneising, O., Krautwurst, S., O'dell, C. W., Richter, A., et al.
636 (2019). Towards monitoring localized CO2 emissions from space: co-located regional CO2
637 and NO2 enhancements observed by the OCO-2 and S5P satellites. *Atmospheric Chemistry*
638 *and Physics*, *19*, 9371–9383. https://doi.org/10.5194/acp-19-9371-2019

639 Richter, A., & Burrows, J. P. (2002). *TROPOSPHERIC NO2 FROM GOME MEASUREMENTS.*
640 *Adv. Space Res* (Vol. 29). Retrieved from www.eIsevier.com/locatelasr

641 Richter, A., Begoin, M., Hilboll, A., & Burrows, J. P. (2011). An improved NO2 retrieval for the
642 GOME-2 satellite instrument. *Atmospheric Measurement Techniques*, *4*(6), 1147–1159.
643 https://doi.org/10.5194/amt-4-1147-2011

644 Romer, P. S., Duffey, K. C., Wooldridge, P. J., Edgerton, E., Baumann, K., Feiner, P. A., et al.
645 (2018). Effects of temperature-dependent NOx emissions on continental ozone production.
646 *Atmospheric Chemistry and Physics*, *18*(4), 2601–2614. https://doi.org/10.5194/acp-18-
647 2601-2018

648 Russell, A. R., Valin, L. C., Bucsela, E. J., Wenig, M. O., & Cohen, R. C. (2010). Space-based
649 constraints on spatial and temporal patterns of NOx emissions in California, 2005-2008.
650 *Environmental Science and Technology*, *44*(9), 3608–3615.
651 https://doi.org/10.1021/es903451j

652 Russell, A. R., Perring, A. E., Valin, L. C., Bucsela, E. J., Browne, E. C., Wooldridge, P. J., &
653 Cohen, R. C. (2011). A high spatial resolution retrieval of NO2 column densities from OMI:
654 Method and evaluation. *Atmospheric Chemistry and Physics*, *11*(16), 8543–8554.
655 https://doi.org/10.5194/acp-11-8543-2011

Shah, V., Jacob, D. J., Li, K., Silvern, R. F., Zhai, S., Liu, M., et al. (2020). Effect of changing NOx lifetime on the seasonality and long-term trends of satellite-observed tropospheric NO2 columns over China. *Atmospheric Chemistry and Physics Discussions*, *20*(3), 1483–1495. https://doi.org/10.5194/acp-2019-670

Souri, A. H., Choi, Y., Jeon, W., Li, X., Pan, S., Diao, L., & Westenbarger, D. A. (2016). Constraining NOx emissions using satellite NO2 measurements during 2013 DISCOVER-AQ Texas campaign. *Atmospheric Environment*, *131*(2), 371–381. https://doi.org/10.1016/j.atmosenv.2016.02.020

Stavrakou, T., Müller, J.-F., Boersma, K. F., De Smedt, I., & van der A, R. J. (2008). Assessing the distribution and growth rates of NOx emission sources by inverting a 10-year record of NO2 satellite columns. *Geophysical Research Letters*, *35*(10). https://doi.org/10.1029/2008GL033521

Timmermans, R., Segers, A., Curier, L., Abida, R., Attié, J.-L., El Amraoui, L., et al. (2019). Impact of synthetic space-borne NO2 observations from the Sentinel-4 and Sentinel-5P missions on tropospheric NO2 analyses. *Atmospheric Chemistry and Physics*, *19*(19), 12811–12833. https://doi.org/10.5194/acp-19-12811-2019

Tzortziou, M. A., Herman, J. R., Cede, A., Loughner, C. P., Abuhassan, N. K., & Naik, S. (2015). Spatial and temporal variability of ozone and nitrogen dioxide over a major urban estuarine ecosystem. *Journal of Atmospheric Chemistry*, *72*(3–4), 287–309. https://doi.org/10.1007/s10874-013-9255-8

Valin, L. C., Russell, A. R., Hudman, R. C., & Cohen, R. C. (2011). Effects of model resolution on the interpretation of satellite NO2 observations. *Atmospheric Chemistry and Physics*, *11*(22), 11647–11655. https://doi.org/10.5194/acp-11-11647-2011

Valin, L. C., Russell, A. R., & Cohen, R. C. (2013). Variations of OH radical in an urban plume inferred from NO2 column measurements. *Geophysical Research Letters*, *40*(9), 1856–1860. https://doi.org/10.1002/grl.50267

Valin, L. C., Russell, A. R., & Cohen, R. C. (2014). Chemical feedback effects on the spatial patterns of the NOx weekend effect: A sensitivity analysis. *Atmospheric Chemistry and Physics*, *14*(1), 1–9. https://doi.org/10.5194/acp-14-1-2014

Vandaele, A. C., Hermans, C., Simon, P. C., Carleer, M., Colin, R., Fally, S., et al. (1998). Measurements of the NO2 absorption cross-section from 42 000 cm−1 to 10 000 cm−1 (238–1000 nm) at 220 K and 294 K. *Journal of Quantitative Spectroscopy and Radiative Transfer*, *59*(3–5), 171–184. https://doi.org/10.1016/S0022-4073(97)00168-4

VanDerA, R. J., Eskes, H. J., Boersma, K. F., van Noije, T. P. C., Van Roozendael, M., De Smedt, I., et al. (2008). Trends, seasonal variability and dominant NOx source derived from a ten year record of NO2 measured from space. *Journal of Geophysical Research Atmospheres*, *113*(4), 1–12. https://doi.org/10.1029/2007JD009021

VanDonkelaar, A., Martin, R. V., Li, C., & Burnett, R. T. (2019). Regional Estimates of Chemical Composition of Fine Particulate Matter using a Combined Geoscience-Statistical Method with Information from Satellites, Models, and Monitors. *Environmental Science & Technology*, acs.est.8b06392. https://doi.org/10.1021/acs.est.8b06392

VanGeffen, J. H. G. M., Eskes, H. J., Boersma, K. F., Maasakkers, J. D., & Veefkind, J. P. (2019). *TROPOMI ATBD of the total and tropospheric NO2 data products*. Retrieved from http://www.tropomi.eu/sites/default/files/files/publicS5P-KNMI-L2-0005-RP-ATBD_NO2_data_products-20190206_v140.pdf

Veefkind, J. P., Aben, I., McMullan, K., Förster, H., de Vries, J., Otter, G., et al. (2012). TROPOMI on the ESA Sentinel-5 Precursor: A GMES mission for global observations of the atmospheric composition for climate, air quality and ozone layer applications. *Remote Sensing of Environment*, *120*(2012), 70–83. https://doi.org/10.1016/j.rse.2011.09.027

Wang, Y., Bechle, M. J., Kim, S.-Y., Adams, P. J., Pandis, S. N., Pope, C. A., et al. (2020). Spatial decomposition analysis of NO2 and PM2.5 air pollution in the United States. *Atmospheric Environment*, 117470. https://doi.org/10.1016/j.atmosenv.2020.117470

Zhao, X., Griffin, D., Fioletov, V., McLinden, C. A., Cede, A., Tiefengraber, M., et al. (2020). Assessment of the quality of TROPOMI high-spatial-resolution NO2 data products in the Greater Toronto Area. *Atmospheric Measurement Techniques*, *13*(4), 2131–2159. https://doi.org/10.5194/amt-13-2131-2020

Zoogman, P., Liu, X., Suleiman, R. M., Pennington, W. F., Flittner, D. E., Al-Saadi, J. A., et al. (2017). Tropospheric emissions: Monitoring of pollution (TEMPO). *Journal of Quantitative Spectroscopy and Radiative Transfer*, *186*(2017), 17–39. https://doi.org/10.1016/j.jqsrt.2016.05.008